Submitted to *GRL* April 2011, this version accepted 13 June, published 25 July 2011. Citation: *Geophysical Research Letters*, 38, L14305, doi:10.1029/2011GL047849, 5 pages, 2011.

Influence of Material Contrast on Fault Branching Behavior

Nora DeDontney[1], James R. Rice[1,2], Renata Dmowska[2]

Material contrasts across faults are a common occurrence, and it is important to understand if these material contrasts can influence the path of rupture propagation. Here we examine models, solved numerically, of rupture propagation through one type of geometric complexity, that of a fault branch stemming from a planar main fault on which rupture initiates. This geometry, with a material contrast across the main fault, could be representative of either a mature strike-slip fault or a subduction zone interface. We consider branches in both the compressional and extensional quadrants of the fault, and material configurations in which the branch fault is in either the stiffer or the more compliant material and configurations with no material contrast. We find that there are regimes in which this elastic contrast can influence the rupture behavior at a branching junction, but there are also stress states for which the branch activation will not depend on the orientation of the mismatch. For the scenarios presented here, both compressional and extensional side branches are more likely to rupture if the branch is on the side of the fault with the more compliant material versus the stiffer material. The stresses induced on the branch fault, by rupture traveling on the main fault, are different for the two orientations of material contrast. We show how the interactions between rupture on the two faults determine which faults are activated.

1. Introduction

Faults often separate dissimilar elastic materials and ruptures are frequently not confined to a single planar fault. Quantifying the ability of rupture on one fault to cause rupture on another fault is needed for proper determination of seismic hazard. Here we examine the rupture path when a rupture, traveling on a bimaterial fault, reaches an intersection with a branching fault.

Fault branching has been observed during strike-slip earthquakes and mature strike-slip faults can have 10's of km of displacement, which can juxtapose differing lithologies. *Ando et al.* [2009] find that branch geometries are common in strike-slip settings at a range of length scales and that geometries with compressional and extensional side branches are equally common (figure 1a).

Branching faults also exist in subduction zones, where there is a strong lithology contrast between the subducting crust and the overriding accretionary prism. *Park et al.* [2002] observed a splay fault in the Nankai trough that branches from the subduction interface and deforms the overriding accretionary prism. Splay faults reach the surface much closer to shore than the subduction interface, so knowledge of their ability to rupture during a major earthquake is important for tsunami hazard. In subduction zones, we focus on faults in the hanging wall, i.e., compressional side branches with the geometry shown in figure 1a.

Rupture typically starts deep on the subduction interface and propagates updip until it reaches an intersection with a splay fault. *Poliakov et al.* [2002] and *Kame et al.* [2003] identified key parameters that affect the rupture path selection including the branch angle, δ (the angle between the main fault and the branch), the rupture velocity, V_r, on the main fault at the branching junction, and the stress state, characterized by Ψ (the angle between the main fault and the most compressive principal stress). High values of Ψ are found around the San Andreas Fault (SAF) [*Zoback et al.*, 1987] and result in stress states in which extensional side faults are favorably oriented for failure. Low values for Ψ are expected in subduction zones and fold-and-trust belt settings, where the subduction interface/detachment dip is shallow, 1-15°, and the maximum compressive stress is approximately horizontal. Low values of Ψ lead to compressional side branches being well oriented for failure.

Dynamic models of rupture through branched geometries have been used to understand the rupture path of strike-slip events with no material contrast [e.g., *Aochi et al.*, 2000; *Oglesby et al.*, 2003; *Duan and Oglesby*, 2007]. Here we show the results of an initial investigation into the role of material contrasts in determining the rupture path selection at the branching junction to assess the likelihood of multi-segment strike-slip ruptures and activation of tsunamigenic splay faults during an earthquake.

2. Model and Methods

Numerical analyses of right-lateral dynamic shear rupture in an elastic medium were conducted using the finite-element code ABAQUS/Explicit. The predefined faults are embedded in 2-dimensional plane strain finite elements and absorbing boundary conditions surround the entire model (see *DeDontney et al.* [2011] and *DeDontney* [2011] for a complete discussion of the model and methods). Two materials are used, and either material can be on each side of the main fault (figure 1b). Material 1 is more compliant than material 2 and also has a slower P and S-wave velocities. In configuration A, material 1 is only on the top half of the model (as shown in figure 1b), in configuration B, material 1 is only on the top half of the model, and in configuration C, material 1 is on both halves of the model.

The model is initially loaded with a uniform stress state with components σ^0_{xx}, σ^0_{yy} and τ^0_{xy}. This stress state is characterized by Ψ, and an S ratio, defined as $S = (\tau_p - \tau_0)/(\tau_0 - \tau_r)$, where τ_0 is the initial shear stress, and τ_p and τ_r are the peak and residual strengths of the fault respectively [*Andrews*, 1976], based on the initially uniform compressive normal stress.

Here we consider both compressional, $0° \leq \delta < 30°$, and extensional side branches, $-30° \leq \delta < 0°$, and use two values for Ψ. *Kame et al.* [2003] show that compressional side branches can be activated for low values of Ψ, and extensional side branches can be activated for high values of Ψ.

[1]Department of Earth and Planetary Sciences, Harvard University, Cambridge, MA, 02138, USA.
[2]School of Engineering and Applied Sciences, Harvard University, Cambridge, MA, 02138, USA.

0094-8276/11/$5.00

Here we use $\Psi = 13^\circ$ and $\Psi = 47^\circ$ to examine compressional and extensional side branches respectively. We specify the rupture velocity at the junction as $V_r = 0.80C_{s1}$ for the extensional branch and $V_r = 0.86C_{s1}$ for the compressional side branch. These values for V_r and Ψ are chosen not for fundamental reasons, but for the range in behaviors that can be exhibited for $1.0 \leq S \leq 3.0$, which we examine, although not all results are shown here. For example, for both potential configurations of materials, $\Psi = 40^\circ$ and $V_r = 0.80C_{s1}$ results in no extensional side branch activation, but $\Psi = 55^\circ$ results in activation of all but one extensional side branch. Therefore, we use $\Psi = 47^\circ$ because it is in the transitional regime and activation is sensitive to parameter choices.

2.1. Material Parameters

We seek to examine both mature strike-slip faults and subduction zones. As a strike-slip example we consider the material contrast across the San Andreas Fault (SAF) with a basement P-wave velocity contrast of 1.09 (5.8 km/s and 6.3 km/s on the southwest and northeast sides, respectively) [*Fuis et al.*, 2003]. Assuming a uniform density and Poissons ratio of $\nu = 0.25$, this results in a shear modulus ratio of 1.19. Studies of the velocity structure in Nankai [e.g., *Takahashi et al.*, 2002], show a representative P-wave contrast of 1.25 between the downgoing and overriding materials (6.5 km/s and 5.2 km/s respectively). If the downgoing plate has a density of 3.0 g/cm^3, which is a reasonable density of gabbro, and the overriding plate has a density of 2.2 g/cm^3, we have a shear modulus contrast of 2.13. We consider a case between these two end members and use a wave speed contrast of 1.11 and a shear modulus contrast of 1.43 (see table 1 for all values).

2.2. Fault Frictional Behavior

We implement a slip weakening formulation [*Ida*, 1972; *Palmer and Rice*, 1973], in which the coefficient of friction, f, decays linearly from a peak static value, $f_s = 0.6$, to a dynamic value, $f_d = 0.12$, over a characteristic amount of slip, D_c. A length scale that arises is the slip weakening zone size, R, and the static slip-weakening zone size is R_0. At low speeds and large S, $R \approx R_0$, and R_0 can be related to D_c for rupture between identical materials [*Palmer and Rice*, 1973]. A resolution of 40 elements in R_0 is used in the vicinity of the faults to ensure that the slip-weakening process is well resolved (where R_0 is calculated for the case of a homogenous material).

We implement a numerical regularization scheme because the bimaterial sliding problem is ill-posed [e.g., *Adams*, 1995]. We use the form

$$\frac{d\tau}{dt} = -\frac{1}{t^*}[\tau - f\sigma_n] \quad (1)$$

where σ_n is the normal stress, positive in compression, and shear strength, τ, evolves towards a residual value over a time scale, t^*, chosen as $t^* = 4\Delta x/C_{s1}$ with Δx the element dimension in the direction of slip. This is a simplified form from that suggested by *Prakash and Clifton* [1993] and *Prakash* [1998], which was shown to have stabilizing properties [*Ranjith and Rice*, 2001; *Cochard and Rice*, 2000].

3. Results and Discussion

3.1. Compressional Side Branches

When the compressional side branch was located in the more compliant material, material 1, the branch is more likely to be activated than if the branch was located in the stiffer material, material 2 (figure 2a). For all material configurations, the same stress states and rupture velocity at the branching junction were used. Material configuration A, with the fault in the more compliant, slower wavespeed material, resulted in complete rupture of the branch for five of the six scenarios shown. Configuration B only resulted in branch activation in two of the six scenarios. If there is no elastic mismatch (configuration C), the branch activation results are very similar to those of material configuration A, but the case of $\delta = 25^\circ$ and $S = 2.2$ (for which there is no branch activation in configuration A) also has branch activation with $L_s = 18.4$. To determine why these differences occur, we examine the stresses around a propagating rupture as well as the stress changes induced on the branch by a rupture propagating past the junction on the main fault. The Coulomb Failure Stress (CFS) accounts for increases in shear stress and decreases in compressional stress, both of which promote failure, through the linear combination $\Delta\text{CFS} = \Delta\tau - f_s\Delta\sigma_n$, where τ and σ_n are calculated for a specified fault plane [*Reasenberg and Simpson*, 1992].

Figure 3a shows the ΔCFS for all material configurations, on all potential fault planes radiating from the rupture tip, at a specified distance, r, which is on the order of R, from the rupture tip. This stress field is shown for $S = 2.2$, around a rupture propagating at $V_r = 0.86C_{s1}$. The rupture and slip velocities are asymmetric for a rupture propagating on a bimaterial interface [e.g., *Andrews and Ben-Zion*, 1997; *Ben-Zion*, 2001; *Harris and Day*, 2005], so this target rupture velocity is reached for different crack lengths, L, depending on the material configuration. We use the distribution in figure 3 as a qualitative assessment of the influence of the material configuration, rather than a comparison of the exact amplitudes of ΔCFS. All configurations show higher increases in CFS on the extensional side of the fault, but those with an elastic mismatch each have a slight relative increase in the stressing level on the side of the fault with the stiffer material. From this figure, it appears that configuration B has the highest stressing of the branch, but configuration B has the least branch activation.

The rupture path selection is dependent not only on the initial stressing due to rupture on the main fault, but also the interactions between ruptures on the two faults (see *Bhat et al.* [2007] for a discussion in the homogenous material case). Therefore we also examine the ΔCFS on a fictional branch as the rupture propagates on the main fault to determine how the main fault rupture alters the stress state on the branch. In figure 3 we consider a branch angle of $\delta = 18^\circ$, for $S = 2.2$, which figure 2a shows to be a case that would have a difference in behavior for the two material configurations with an elastic mismatch. At time 1, the rupture is at the fictional branch junction, and this is when the associated high stresses nucleate rupture on the branch. At times 2 and 3, the rupture has propagated past the junction a distance specified in figure 3b.

At time 1, all configurations show an increase in CFS at the junction and over the length of the branch. The stressing near the junction is highest for configuration B, consistent with the distribution seen in figure 3a, but this configuration has little branch activation. This is due to the stress field as the rupture propagates by on the main fault (times 2 and 3). Configuration B shows a lower level of sustained stressing, compared to configurations A and C, meaning that configuration B does not see high stresses for a long enough duration for complete slip weakening of the branch to take place. The trough in Coulomb stressing shadows the branch fault, and should inhibit branch fault activation. Configuration A has the shallowest trough so the main fault rupture is unable to inhibit rupture on the branch and the main fault rupture dies out. However, configuration C has the deepest trough and yet branch activation occurs. This indicates that the

trough is less important than the sustained high stressing, and we must also consider the effect of branch fault rupture on the main fault [*Bhat et al.*, 2007]. For $\delta = 20^\circ$, rupture on the main fault dies out more quickly for configuration C than configuration A, due to a larger shadow on the main fault from rupture propagating on the branch. Therefore, in configuration C, the branch shadows the main fault before the main fault is able to shadow the branch, so the branch is activated.

3.2. Extensional Side Branches

There is also a change in the branching behavior for extensional side branches, and once again the branch is more likely to be activated if it is in the more compliant material 1 (figure 2b). If there is no material contrast, the branching behavior is intermediate to the cases with a contrast; for $S = 1.4$, both the main fault and branch fault are activated for all branch angles, and for $S = 2.2$, there is no branch activation ($L_s < 7.0$). For the cases shown here, the extensional branch in the stiffer material is never taken, but, as noted, there are stress states and rupture velocities for which this branch is taken.

An examination of the stress field around the propagating crack tip for $S = 1.4$ and $V_r = 0.80C_{s1}$ and on a fictional branch angle of $\delta = -18^\circ$, shows only subtle differences between all the material configurations (figure 4), and the stress distribution is very similar for $S = 2.2$. While the differences are small, they are able to result in very different outcomes and it is a good illustration of the complexity of the interactions between the two faults in determining the rupture path selection. The initial stressing levels, at time 1, are quite comparable for all material configurations. At times 2 and 3, configuration B has the smallest stress shadow on the branch, allowing for branch rupture to always occur. Additionally as rupture begins to propagate on the branch, this configuration has the largest shadowing of the main fault, and this slows down the main fault rupture and allows the branch rupture establish itself. Configuration A does not show complete branch activation but as rupture tries to propagate on the branch, this configuration has the smallest shadowing of the main fault. Therefore, the main fault rupture dominates and inhibits rupture of the branch. Configuration C has an intermediate shadowing of the main fault, and therefore has an intermediate fault branching behavior.

4. Conclusions

An elastic material mismatch across a fault is able to influence the dynamic rupture path selection through a branching junction. The stresses around a propagating crack tip are dependent upon the material configuration. Additionally, the stress changes induced on the branch fault, due to rupture on the main fault, are influenced by the material contrast. The interactions between rupture on the two faults are complex and play an important, if subtle, role in the branch activation. For a compressional side branch, it is clear that the stresses induced on the branch due to the rupture propagation on the main fault are strongly influencing the rupture behavior on the branch. For extensional side branches, the differences in induced stresses are subtle, and it is also important to consider the effects of the branch fault rupture on the main fault. Both compressional and extensional side branches are more likely to rupture if the branch is on the side of the fault with the more compliant material. The elastic mismatch does not preclude branch faults from rupturing if they are in the stiffer material, but they are less likely to be taken than if the branch was in a compliant material, all else being equal. This result is especially important for splay fault geometries in subduction zones. Mega-splay faults cut through the overriding accretionary prism, which is more compliant than the subducting oceanic crustal material. From that point of view, tsunamigenic splay faults are likely to rupture coseismically.

Acknowledgments. This research was supported by National Science Foundation (NSF)EAR award 0809610 and by the Southern California Earthquake Center (SCEC); SCEC is funded by NSF Cooperative Agreement EAR-0529922 and USGS Cooperative Agreement 07HQAG0008. The SCEC contribution number for this paper is 1487. We are grateful to Harsha Bhat, Elizabeth Templeton and Robert Viesca for their initial guidance in setting up these problems.

References

Adams, G. G. (1995), Self-excited oscillations of two elastic half-spaces sliding with a constant coefficient of friction, *J. Appl. Mech.*, *62*, 867–872.

Ando, R., B. E. Shaw, and C. H. Scholz (2009), Quantifying natural fault geometry: Statistics of splay fault angles, *Bull. Seis. Soc. Am.*, *99*(1), 389–395, doi:10.1785/0120080942.

Andrews, D. J. (1976), Rupture velocity of plane strain shear cracks, *J. Geophys. Res.*, *81*(32), 5679–5687.

Andrews, D. J., and Y. Ben-Zion (1997), Wrinkle-like slip pulse on a fault between different materials, *J. Geophys. Res.*, *102*(B1), 553–571.

Aochi, H., E. Fukuyama, and M. Matsuura (2000), Selectivity of spontaneous rupture propagation on a branched fault, *Geophys. Res. Lett.*, *27*(22), 635–638.

Ben-Zion, Y. (2001), Dynamic ruptures in recent models of earthquake faults, *J. Mech. Phys. Solids*, *49*, 2209–2244.

Bhat, H. S., M. Olives, R. Dmowska, and J. R. Rice (2007), Role of fault branches in earthquake rupture dynamics, *J. Geophys. Res.*, *112*(B11), doi:10.1029/2007JB005027.

Cochard, A., and J. R. Rice (2000), Fault rupture between dissimilar materials: Ill-posedness, regularization and slip-pulse response, *J. Geophys. Res.*, *105*(B11), 25,891–907.

DeDontney, N., J. R. Rice, and R. Dmowska (2011), Finite element modeling of branched fault ruptures including off-fault plasticity, *submitted to BSSA*.

DeDontney, N. L. (2011), Branch faulting in subduction and strike-slip settings, Ph.D. thesis, Harvard Univ.

Duan, B., and D. D. Oglesby (2007), Nonuniform prestress from prior earthquakes and the effect on dynamics of branched fault systems, *J. Geophys. Res.*, *112*, B05,308, doi:10.1029/2006JB004443.

Fuis, G. S., et al. (2003), Fault systems of the 1971 San Fernando and 1994 Northridge earthquakes, southern California: Relocated aftershocks and seismic images from LARSE II, *Geology*, *31*(2), 171–174.

Harris, R. A., and S. M. Day (2005), Material contrast does not predict earthquake rupture propagation direction, *Geophys. Res. Lett.*, *32*, L23,301, doi:10.1029/2005GL023941.

Ida, Y. (1972), Cohesive force across the tip of a Longitudinal-Shear crack and Griffith's specific surface energy, *J. Geophys. Res.*, *77*(20), 3796–3805.

Kame, N., J. R. Rice, and R. Dmowska (2003), Effect of prestress state and rupture velocity on dynamic fault branching, *J. Geophys. Res.*, *108*(B5), 2265, doi:10.1029/2002JB002189.

Oglesby, D. D., S. M. Day, Y.-G. Li, and J. E. Vidale (2003), The 1999 Hector Mine earthquake: The dynamics of a branched fault system, *Bull. Seis. Soc. Am.*, *93*(6), 2459–2476.

Palmer, A. C., and J. R. Rice (1973), Growth of slip surfaces in progressive failure of over-consolidated clay, *Proceedings of the Royal Society of London Series A-Mathematical Physical and Engineering Sciences*, *332*(1591), 527–548.

Park, J.-O., T. Tsuru, S. Kodaira, P. R. Cummins, and Y. Kaneda (2002), Splay fault branching along the Nankai subduction zone, *Science*, *297*, 1157–1160.

Poliakov, A. N. B., R. Dmowska, and J. R. Rice (2002), Dynamic shear rupture interactions with fault bends and off-axis secondary faulting, *J. Geophys. Res.*, *107*(B11), 2295, doi: 10.1029/2001JB000572.

Prakash, V. (1998), Frictional response of sliding interfaces subjected to time varying normal pressures, *J. of Tirbol.*, *120*, 97–102, doi:10.1115/1/2834197.

Prakash, V., and R. J. Clifton (1993), Time resolved dynamic friction measurements in pressure-shear, in *Experimental Techniques in the Dynamics of Deformable Solids*, edited by A. K. T. Ramesh, pp. 33–48, Appl. Mech. Div., Am. Soc. of Mechanical Eng., Ney York.

Ranjith, K., and J. R. Rice (2001), Slip dynamics at an interface between dissimilar materials, *J. Mech. Phys. Solids*, *49*, 341–361.

Reasenberg, P. A., and R. W. Simpson (1992), Response of regional seismicity to the static stress change produced by the Loma Prieta Earthquake, *Science*, *255*(5052), 1687–1690, doi: 10.1126/science.255.5052.1687.

Takahashi, N., et al. (2002), Seismic structure of western end of the Nankai trough seismogenic zone, *Journal Geophys. Res.*, *107*, B102,212, doi:10.1029/2000JB000121.

Zoback, M. D., et al. (1987), New evidence on the state of stress of the San Andreas fault system, *Science*, *238*(4830), 1105–1111.

Nora DeDontney, Dept. of Earth and Planetary Sciences, Harvard Univ., 20 Oxford St., Cambridge MA 02138, USA. (ndedontn@fas.harvard.edu)

James R. Rice, School of Engineering and Applied Sciences and Dept. of Earth and Planetary Sciences, Harvard Univ., Cambridge MA 02138, USA.

Renata Dmowska, School of Engineering and Applied Sciences, Harvard Univ., Cambridge MA 02138, USA.

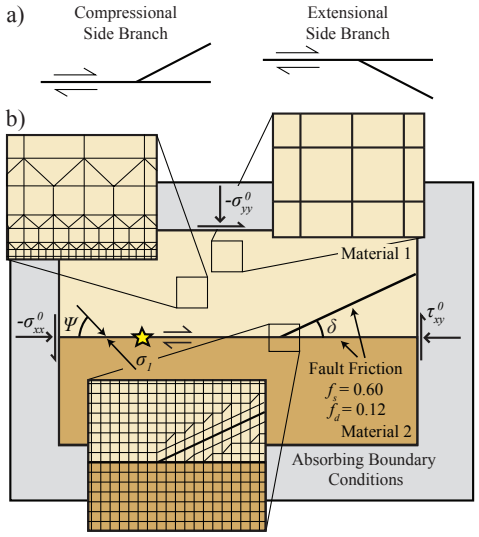

Figure 1. (a) Definition of compressional and extensional side branches. (b) Finite element model setup showing mesh geometry. There can be a material contrast across the main fault (contrast shown in configuration A) or material 1 is on both sides of the fault (configuration C).

Table 1. Material Parameters

ρ_1, ρ_2	Density	2600, 3000 kg/m^3
ν_1, ν_2	Poisson's ratio	0.25, 0.25
C_{p1}, C_{p2}	P wave speed	5500, 6100 m/s
C_{s1}, C_{s2}	S wave speed	3175, 3521 m/s
E_1, E_2	Young's modulus	65.5, 93.0 GPa
G_1, G_2	Shear modulus	26.2, 37.2 GPa
R_0	Slip weakening zone size	40 m
f_s	Static friction	0.6
f_d	Dynamic friction	0.12
D_c	Slip weakening length	62 mm
t^*	Regularized time scale	1.26e-3 s

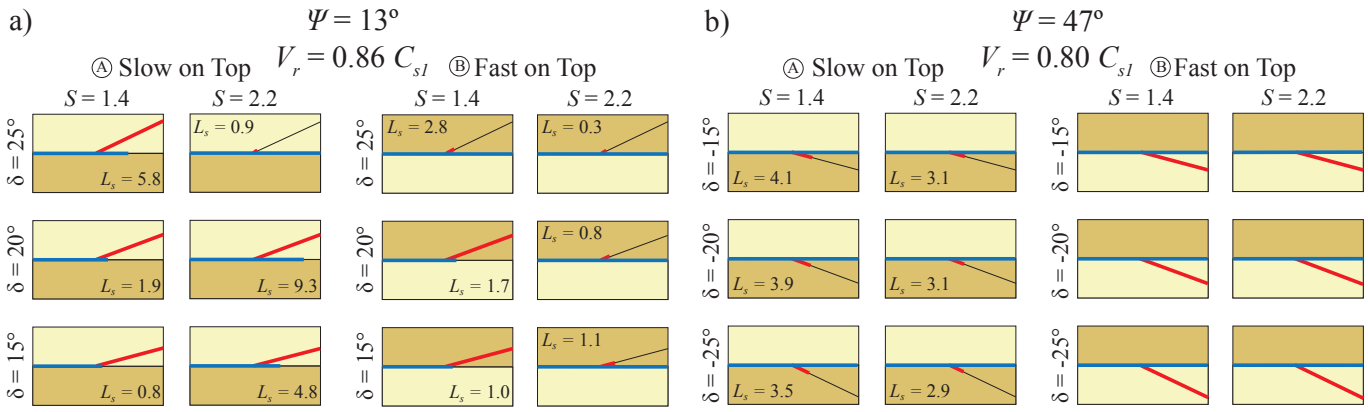

Figure 2. Branch activation results denoted with main fault activation in blue and branch fault activation in red. Both compressional side branches (a) and extensional side branches (b) are more likely to rupture when the branch is in a more compliant material. L_s is the distance a failed rupture propagated on the fault, normalized by R_0.

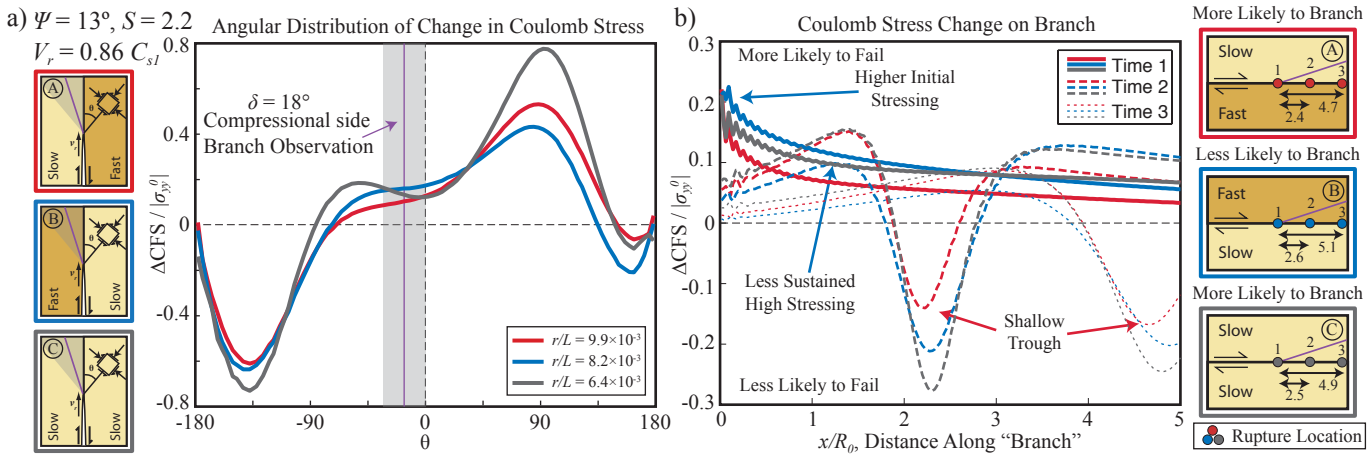

Figure 3. (a) Change in Coulomb stress distribution around a propagating rupture tip, for the parameters in figure 2, shows highest initial branch stressing for configuration B. Location of compressional side branch observation line also shown. (b) Change in Coulomb stress on noted observation branch due to rupture propagation on the main fault. Stress distribution is different for the three configurations and results in little branch activation for configuration B.

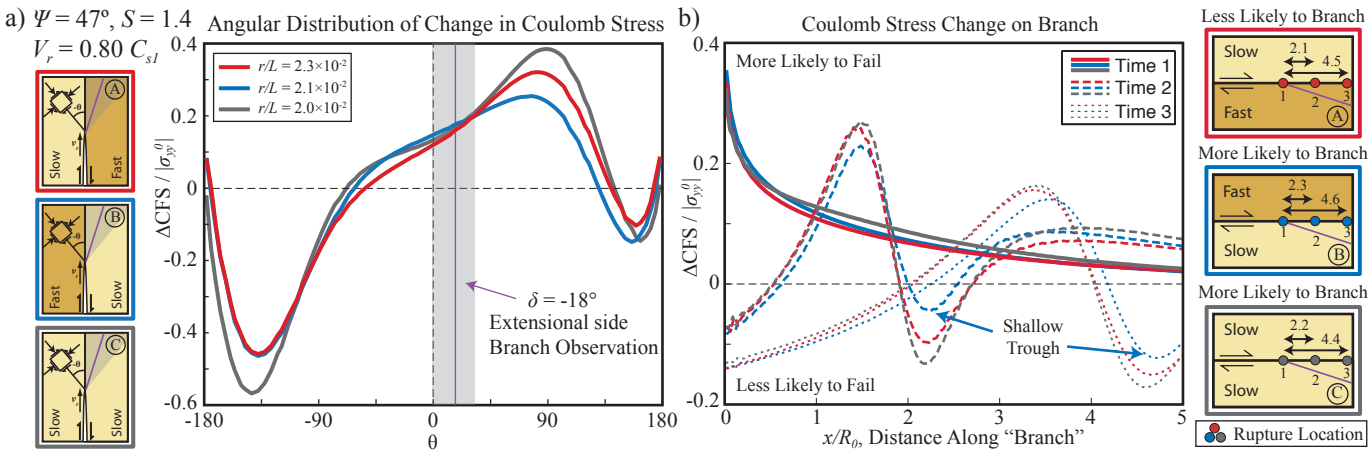

Figure 4. Same as figure 3, but for extensional side branch. There are only small changes in the stress distribution that can lead to different observations of branch activation due to the interaction of the two rupture tips.